

Galaxy Image Deconvolution for Weak Gravitational Lensing with Physics-informed Deep Learning


Tianao Li (李天骢),¹★ Emma Alexander²†

¹Department of Electronic Engineering, Tsinghua University, Haidian District, Beijing 100084, P.R.China

²Department of Computer Science, Northwestern University, Evanston, IL 60208, USA

Accepted XXX. Received YYY; in original form ZZZ

ABSTRACT

Removing optical and atmospheric blur from galaxy images significantly improves galaxy shape measurements for weak gravitational lensing and galaxy evolution studies. This ill-posed linear inverse problem is usually solved with deconvolution algorithms enhanced by regularisation priors or deep learning. We introduce a so-called "physics-based deep learning" approach to the Point Spread Function (PSF) deconvolution problem in galaxy surveys. We apply algorithm unrolling and the Plug-and-Play technique to the Alternating Direction Method of Multipliers (ADMM) with a Poisson noise model and use a neural network to learn appropriate priors from simulated galaxy images. We characterise the time-performance trade-off of several methods for galaxies of differing brightness levels, showing an improvement of 26% (SNR=20)/48% (SNR=100) compared to standard methods and 14% (SNR=20) compared to modern methods. 

Key words: techniques: image processing - methods: data analysis - galaxies: general.

1 INTRODUCTION

Images captured by real-world systems are degraded by nonidealities in the atmosphere, optics, and sensors. Processing images to correct these effects can significantly reduce errors in physical measurements drawn from astronomical images, such as the galaxy shape estimation used in cosmological weak lensing analysis to advance our understanding of cosmological models, the relationship between visible and dark matter, and cosmological-scale gravity (Kaiser et al. 1994; Bartelmann & Schneider 2001; Mandelbaum et al. 2015; Mandelbaum 2018). Conventionally, these nonidealities are modelled by convolution with a blur kernel called the Point Spread Function (PSF), followed by noise. Many computer vision algorithms have been developed to solve this ill-posed linear inverse problem, known as deconvolution. Here, we characterise the improvements that can be made to shear estimation through several deconvolution approaches, with a focus on a data-driven unrolled optimisation.

Two classic deconvolution algorithms still in widespread use are inverse filtering, also known as *Fourier division* (Stroke & Zech 1967), and the iterative *Richardson-Lucy algorithm* (Richardson 1972; Lucy 1974), which optimizes the image estimate using gradient descent with an adaptive step size. As we will reiterate in this paper, inverse filtering notoriously amplifies noise, while the Richardson-Lucy algorithm is not regularised and converges slowly to a noisy solution (Dey et al. 2004). Note that Weiner deconvolution (Wiener 1949) is also used, but this approach is designed to remove Gaussian additive noise. Poisson noise is a significantly more accurate model for the sensor noise characteristics in photon-starved applications like astronomical imaging (Harman et al. 2011), so deconvolution

techniques based on Gaussian noise models will not be considered here. These shortcomings make it clear that better deconvolution methods are needed for fast and accurate shear estimation.

With the recent flourishing of deep learning, such algorithms have been developed. In computer vision, so-called physics-based machine-learning combines an explicit forward model of the image formation process with data-driven regularisation. Notably, Sureau et al. (2020) introduced two such deconvolution approaches enhanced by deep learning: *Tikhonet*, which post-processes the results of Tikhonov deconvolution with a deep neural net, and *ADMMNet*, an iterative deconvolution framework with learned hyperparameters. ADMMNet is based on the Alternating Direction Method of Multipliers (ADMM, Boyd et al. 2011), which finds the maximum-a-posteriori estimate of the ground truth image by alternating between tractable subproblems. After each subproblem, estimates are updated with a variable step size, where the optimal step sizes depend on the generally-unknown prior distribution of the dataset. ADMMNet takes advantage of the Plug-and-Play approach (Chan et al. 2016), in which the subproblems are seen to correspond to alternating deblurring and denoising steps. This modular structure is exploited by including an off-the-shelf denoiser (typically a deep neural network) in place of the standard denoising step, for more accurate data-driven priors within the context of an interpretable and well-studied optimisation problem. Unfortunately, even with these learned denoisers, the other subproblems in ADMMNet are still optimised for Gaussian noise, as is Tikhonov deconvolution. Both Tikhonet and ADMMNet show significant improvements over classical methods for bright galaxies, but fail in low SNR settings due to this built-in assumption of Gaussian noise.

We evaluate a plug-and-play ADMM network with two important improvements: algorithm unrolling and a Poisson noise model. In an "unrolled" or "unfolded" iterative optimisation, the iteration count is

★ E-mail: lukeli0425@gmail.com

† E-mail: ealexander@northwestern.edu

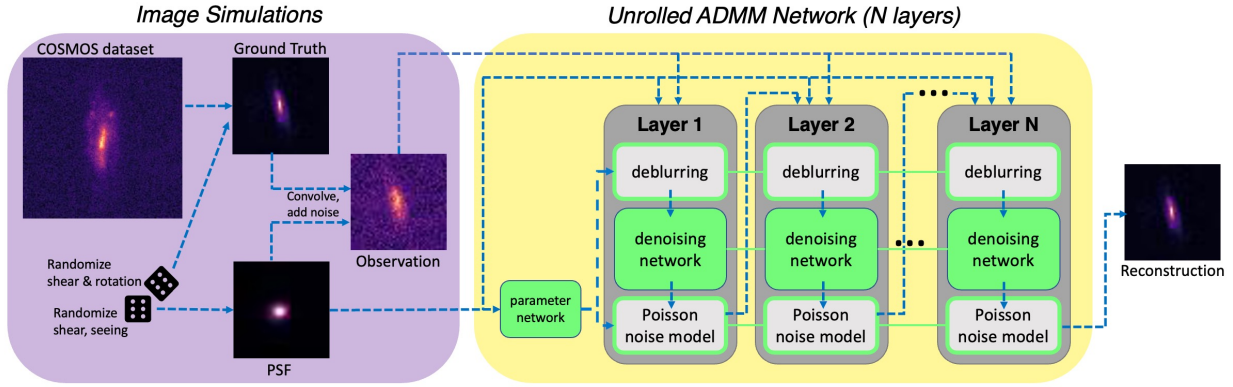


Figure 1. Overview of the image processing pipeline. *Image simulations:* we simulated galaxy images for the upcoming LSST ground-based sky survey by modifying galaxy images from the COSMOS Dataset with the modular galaxy image simulation toolkit Galsim. The raw images are scaled to a target flux value and randomly sheared and rotated before being spatially downsampled by a factor of 4 (16x in area) to a pixel scale of 0.2 arcsec. PSFs consisting of both atmospheric and optical components were generated with realistic seeing and shear distributions. The downsampled galaxy is convolved with the PSF and Poisson shot noise and Gaussian read noise are added to the image. *Model:* we unrolled Plug-and Play ADMM with a Poisson likelihood into an N-layer neural network, with separate networks trained for $N = 1, 2, 4, 8$. Light grey boxes denote fixed computations while green boxes are neural networks (a small convolutional neural network for hyperparameter estimation and a ResUNet for denoising). Green outlines indicate the use of a few trained parameters in the fixed computations and horizontal green lines show that weights are shared across network layers.

fixed a priori and each layer of a neural network performs one stage of the optimisation. Layers contain fixed computations reflecting built-in knowledge (the image formation model) as well as optimisation parameters (the denoising network and step size hyperparameters) that are treated as learnable weights. This approach allows efficient, data-driven fine-tuning of interpretable and well-analysed optimisation methods. [Sanghvi et al. \(2022\)](#) derive the appropriate ADMM updates for Poisson noise, removing the issue seen in ADMMNet by introducing a Poisson-specific update step after the denoising network. Fig. 1 shows the proposed network architecture, with fixed computations shown in light grey and learned parameters indicated in green. The green boxes are small neural networks, green outlines denote the use of trained hyperparameters, and horizontal green lines indicate that learned weights are identical across layers.

In this paper, we benchmark classical and modern deconvolution methods on realistic simulated data for ellipticity error and compute time across several noise conditions, showing that unrolled plug-and-play ADMM with a Poisson noise model, not previously applied to astronomical images, outperforms former methods comprehensively. We also provide source code and trained weights of the suggested model. Our user friendly framework allows one to easily simulate their own data set and train the model under their settings. Our code and tutorials are all available on our GitHub repository.

2 EXPERIMENTS

2.1 Image Simulations

To benchmark classical methods and train our network, clean ground truth images must be paired with realistic PSFs and noisy blurred images. We created our dataset by simulating ground-based observations with the modular galaxy image simulation toolkit Galsim ([Rowe et al. 2015](#)) and the COSMOS Real Galaxy Dataset ([Mandelbaum et al. 2012](#)).

The image simulation process is illustrated in Fig. 1 and was based on the upcoming Legacy Survey of Space and Time (LSST, [Ivezić et al. 2019](#)). Raw images were picked randomly from the COSMOS dataset, added to a sky level of 1000 ADU/arcsec², and their brightness was scaled corresponding to the SNR of interest

(for a total flux of $\sim 35,000$ ADU for SNR=100, $\sim 6,000$ ADU for SNR=20, and $\sim 3,000$ ADU for SNR=10, based on the definition $SNR = \text{flux} / \sqrt{\text{flux} + \text{sky level} \times \text{area} + \text{read noise}^2}$). These images were then randomly sheared (uniform distribution of $[0, 0.25]$) and rotated (uniform distribution of $[0, 2\pi]$) before being downsampled to the pixel scale of the LSST (from 0.05 to 0.2 arcsec) to provide ground truth images.

We then applied both atmospheric and optical blurring. The atmospheric PSFs were simulated with the Kolmogorov function, whose seeing (FWHM) was sampled from a normal distribution with mean 0.67 and variance 0.18, consistent with site measurements ([Claver et al. 2006](#)). To simulate the atmospheric variation that leads to shape noise, we added shear (distribution details) and rotation (distribution details) to the Kolmogorov functions. Our optical PSFs were simulated using Galsim, using the LSST diameter for diffraction and built-in ranges for obscuration, defocus, coma aberration and astigmatism. The two PSF components were convolved to get the overall PSF, which is saved for training and testing. The ground truth image was then convolved with this simulated PSF, before Poisson shot noise and Gaussian read noise with a standard deviation of 5 ADUs per pixel was added to simulate the observed image.

2.2 Network Training

We follow [Sanghvi et al. \(2022\)](#)'s network structure and training, using multi-scale L1 loss for 50 epochs. A separate network was trained for each iteration count ($N=1, 2, 4, 8$). ResUNet ([He et al. 2016](#)) serves as the plugin denoiser (17,007,744 parameters), introducing skip connections in the neural network to avoid the problem of vanishing or exploding gradients as the network gets deeper with the increase of iterations. A CNN (802,36 parameters) was trained to learn the step size hyperparameters. We use their implementation of the network in the open source machine learning framework PyTorch, with which we also provide tools for dataset generation and benchmarking.

2.3 Performance across SNR levels

We tested the suggested method at different SNR levels and compared its performance to other algorithms. Sample images deconvolved by

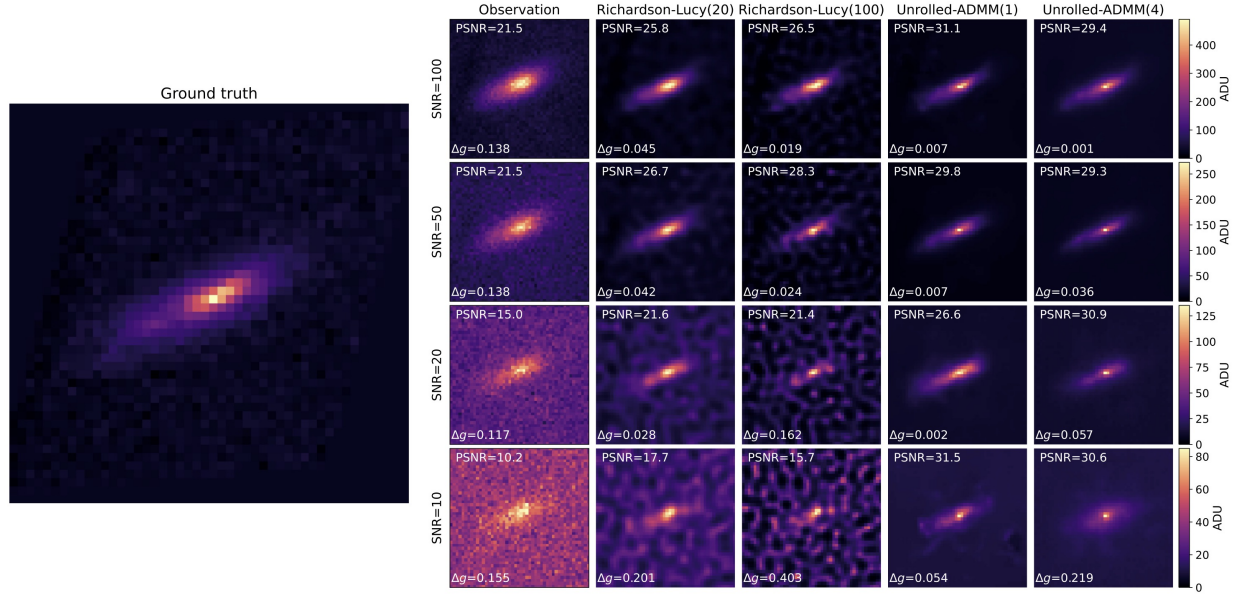


Figure 2. An illustration of performance at multiple SNR levels. The size of each image is 48x48 pixels and each row corresponds to a different SNR level (see brightness in ADU on color bars to the right). PSNR and ellipticity errors are given for each reconstructed image. Columns from left to right: simulated observation, Richardson-Lucy deconvolution with 20 and 100 iterations, and unrolled ADMM with 1 and 4 iterations. Richardson-Lucy gradually fails with the decrease of SNR while the suggested unrolled-ADMM remains effective across SNR levels.

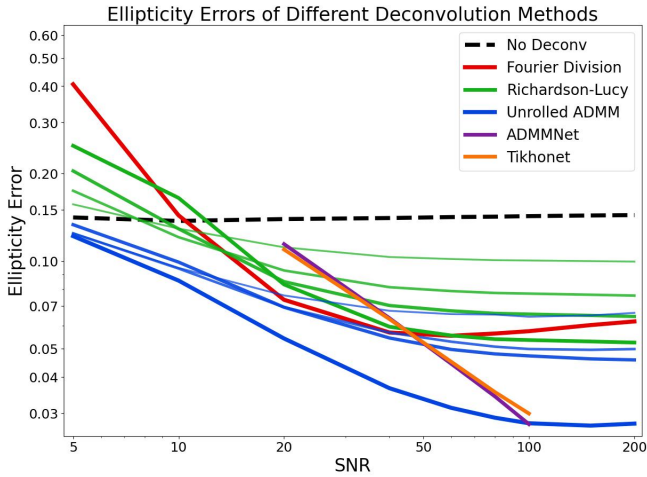


Figure 3. Average ellipticity errors at multiple SNR levels. As all the methods gradually fail with the decrease of SNR, our 8-iteration unrolled ADMM network presents the best performance across SNR levels. Other modern methods perform well on bright images only. Line width indicates number of iterations for Richardson-Lucy (10,20,30,50) and ADMM (1,2,4,8), with thicker lines corresponding to more iterations. The crossings between lines of the same algorithm reveal that a large iteration level amplifies the noise at low SNR levels.

each of the algorithms are shown in Fig. 2. As the SNR decreases, the Richardson-Lucy algorithm results in noisier reconstructions that are gradually submerged in the noisy patterns in the background. In contrast to the failure of Richardson-Lucy, the suggested method not only cleans the noisy background but also retains the shape of the background galaxy, so it provides an effective reduction of systematic error for weak lensing shear estimation. These improvements can be seen in the PSNR for each deconvolved image, reflecting overall

image reconstruction quality, but more importantly they are also seen in the ellipticity estimation error. This error, for which we use reduced shear (Bartelmann & Schneider 2001) calculated with the FPFS estimator (Li et al. 2018), is a more significant evaluation metric because it directly impacts weak lensing measurements.

We characterise the ellipticity error of each method across a dataset of 10000 simulated galaxy images for 9 SNR levels from 5 to 200. We also tested the Richardson-Lucy algorithm and the built-in robust Fourier division method of FPFS as comparisons, and include reported errors from Tikhonet and ADMMNet for comparison. Fig. 3 shows the SNR response curve.

All methods have reduce the ellipticity error for bright galaxies (high SNR), but Richardson-Lucy and Fourier division results are worse than doing no deconvolution when the SNR is lower than 10. The ellipticity error of the two modern methods increases significantly with the decrease of SNR. This falloff is particularly significant given the high prevalence of dim galaxies anticipated in the LSST data, the majority of which will have SNR < 20 (Abell et al. 2009). In terms of ellipticity error and robustness to Poisson shot noise, the best algorithm tested is the 8-iteration unrolled ADMM.

It is worth noting that a high iteration level does not always lead to better reconstructions. This can be seen in the low SNR regime for both the Richardson-Lucy algorithm and the unrolled ADMM, shown in Fig. 3 as the crossing of lines around an SNR of 10. A possible cause is that large-iteration algorithms are over-computing on noisy data, magnifying shape error at low SNR levels. In Fig. 2 the effect of large iterations can be seen as a sharpening of noise artefacts in the background for Richardson-Lucy and an erosion of the galaxy edges for ADMM.

2.4 Time-Performance Trade-off

We tested the classic and Poisson ADMM methods from the perspective of time and performance, aiming to provide the best choice of algorithm and parameters for various demands. ADMMNet and Tikhonet were excluded from this analysis due to their reliance

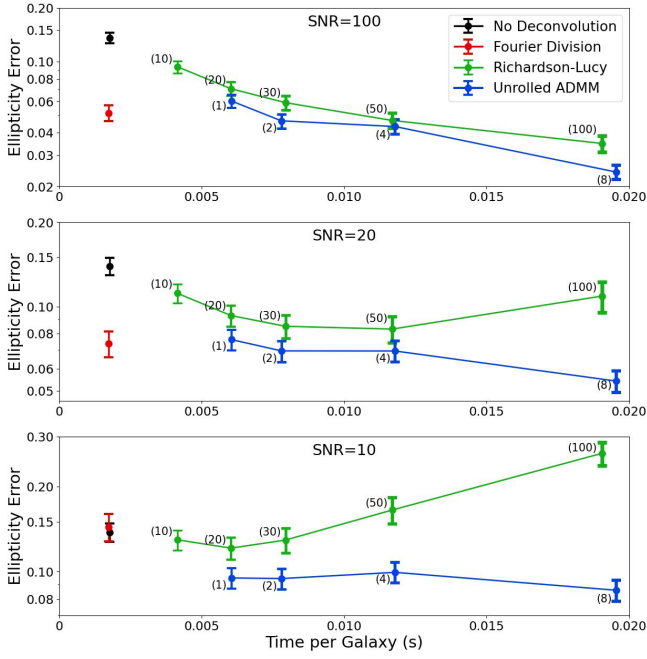


Figure 4. Ellipticity error curve with respect to time at different SNR levels. High-iteration Unrolled ADMM shows higher performance and lower variance across SNR levels, but takes more time. The three panels correspond to SNR of 100, 20 and 10. Error bars show 10x standard error and parentheses indicate number of iterations. Timing and variance were unavailable for ADMMNet and Tikhonet, so they have been excluded.

on libraries that are no longer well supported (TensorFlow v1). We present a trade-off between time and ellipticity error at SNR levels of 10, 20 and 100 on 10000 galaxies in the test dataset, shown in Fig. 4. Error bars show 10x the standard error of the absolute ellipticity errors to assess the stability of the algorithms.

As before, all methods reduce ellipticity error substantially in bright galaxies with an SNR of 100. Ellipticity error and variance decrease with more iterations for these bright galaxies, but as the SNR decreases, Fourier division and Richardson-Lucy rapidly degrade. Over-computation in Richardson-Lucy appears as an increase in error and variance across iteration level in the SNR=10 case, while ADMM retains its performance across iteration levels. Eight-iteration ADMM leads to the lowest errors in all cases but takes nearly 0.02 seconds per image to run on GPU. For time-constrained applications, Fourier division is appropriate under high SNR conditions but low-iteration ADMM should be used for dim galaxies.

2.5 Robustness to Systematic Errors in PSF

In real-world observations, PSFs at the center of the galaxies are calculated through interpolation from PSFs measured at stars, yet the spatial variance of the PSF across the field of view is often difficult to model (Terry et al. 2022). As a result, interpolation cannot precisely reconstruct the effective PSF at the center of galaxies. This requires the subsequent deconvolution algorithm to be robust to systematic errors in the PSFs.

Errors in PSF shape and size result in additive and multiplicative shear biases (Mandelbaum 2018). In our PSF model, these two types of systematic errors correspond to errors in the PSF shear and the full-width half maximum (FWHM) of the Kolmogorov function, i.e., the atmospheric seeing. To test the robustness of the suggested

method to PSF noise, we characterized the ellipticity errors caused by systematic errors (i.e. model mismatch) between the PSF used for image formation and the PSF provided to the deconvolution algorithms. Fig. 5 shows these errors, with an illustration of the type and level of error shown in the cartoon PSFs below the plots. As expected, all algorithms suffer under PSF error. Under reasonable PSF errors, high-iteration ADMM is still the best algorithm, but performance degrades sharply for large mistakes in PSF shape and size. Due to this sensitivity to model mismatch, iteration number should be reduced when high errors in PSF estimation are expected.

3 DISCUSSION

The proposed method could be further improved in several ways. First, the Poisson noise model built into our ADMM update steps does not perfectly fit the actual case, where both the Poisson shot noise and CCD read noise exist. A possible approach is to treat the noise as a combined Poisson and Gaussian noise, as in Ikoma et al. (2018). Second, the network is trained with a multi-scale L1 loss, which might not best preserve the shape of the galaxies. An interesting study would be to train our network with the new loss function adopted by Nammour et al. (2021, 2022) and to examine whether this technique could enhance the performance of unrolled ADMM. It is also suggested that PSF interpolation be included in the pipeline and combined with low-rank deconvolution used in Farrens et al. (2017) and Yanny et al. (2020). Our simulated data can be improved with more accurate optical models for the LSST PSF (Terry et al. 2022) and more realistic generative models such as Peterson et al. (2005), which will only improve once observations begin.

An interesting phenomenon emerging in our experiments was the loss of performance for high iteration counts at low SNR or large PSF systematic noise levels. That is, in the easy case where SNR is high and PSFs are accurately estimated, both Richardson-Lucy and unrolled ADMM perform better with more iterations, while under harsh conditions, a large number of iterations tend to aggravate the failure of these algorithms by amplifying the noise in the image or PSF model. This over-computation of iterative algorithms results in the line crossings in Fig. 3 and 5. Detecting these conditions in the data and changing to a lower-iteration network dynamically could significantly boost robustness.

4 CONCLUSIONS

Modern deconvolution methods improve the appearance of images, but their reliance on deep learning often fails to meet scientific standards of rigor and interpretability. Here, we have simulated galaxy images to train a specific subset of the parameters in a well-studied optimisation method. In comparison with traditional methods, the suggested model is more robust and effective because it denoises images with a neural network that represents a much more realistic prior. Meanwhile, it is also more interpretable and training-data-efficient than pure deep learning approaches because an image formation model is directly incorporated. Importantly, the optimisation steps are based on a Poisson noise model rather than the Gaussian noise model used in previous ADMM-based approaches, leading to better performance on dim images.

We tested the suggested method on data simulated with realistic galaxy images, and compared its performance to classical and modern methods in terms of ellipticity error and variance, time consumption, the robustness to systematic PSF noise, and examined the influence of SNR and iteration count. Our experiments showed that 8-iteration unrolled ADMM with built-in Poisson noise model gives

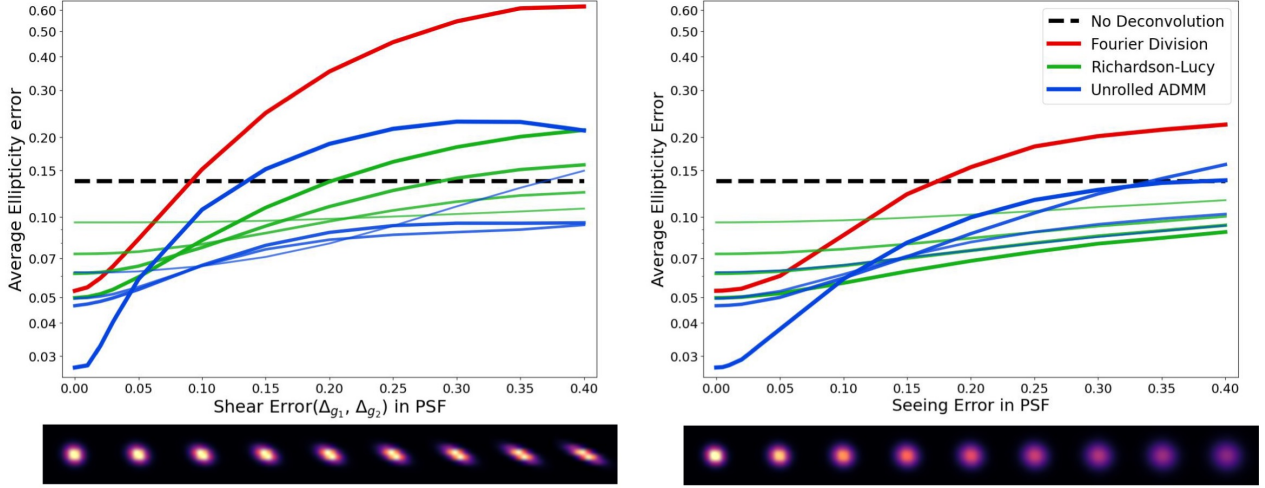


Figure 5. The response curves of ellipticity error as a function of systematic errors in the PSF. The left panel corresponds to shear error in the PSF while the right corresponds to size (FWHM, i.e. the atmospheric seeing) error in the PSF. Line width indicates number of iterations for Richardson-Lucy (10,20,30,50) and ADMM (1,2,4,8). The cartoon bar under the horizontal axis gives an visual indication of the systematic error in PSF. Fourier division and iterative algorithms with high iteration counts show higher sensitivity to model mismatch.

the most accurate and stable ellipticity measurements across SNR levels, but at the cost of elevated compute time.

Because image statistics and computational resources vary across applications and observational conditions, the networks we trained will not be the best method for every galaxy image deconvolution problem. Our simulations were modelled on a specific instrument currently in development, and deviations from these parameters will reduce performance. Because of this, we provide an open-source, user-friendly code base for generating and retraining on simulated datasets for any galaxy image deconvolution problem. Simulation results allow researchers to develop and select the most suitable algorithm for their performance and speed needs.

ACKNOWLEDGEMENTS

We would like to thank Adam Miller, Jason Wang, and Keming Zhang for their valuable advice, and the Computational Photography Lab (esp. Aniket Dashpute) at Northwestern University for support of computational resources.

DATA AVAILABILITY

Our GitHub repository (<https://github.com/Lukeli0425/Galaxy-Deconvolution>) includes the code needed to regenerate the simulated data, as well as a link to the dataset we used. We also provide the suggested unrolled ADMM model with trained weights along with tutorials for using it, allowing a convenient deconvolution with the suggested method for further research.

REFERENCES

Abell P. A., et al., 2009, arXiv preprint arXiv:0912.0201
 Bartelmann M., Schneider P., 2001, *Physics Reports*, 340, 291
 Boyd S., Parikh N., Chu E., Peleato B., Eckstein J., et al., 2011, *Foundations and Trends® in Machine learning*, 3, 1
 Chan S. H., Wang X., Elgendy O. A., 2016, *IEEE Transactions on Computational Imaging*, 3, 84
 Claver C. F., et al., 2006, in *American Astronomical Society Meeting Abstracts*. pp 86–18
 Dey N., Blanc-Féraud L., Zimmer C., Kam Z., Olivo-Marin J.-C., Zerubia J., 2004, in *2004 2nd IEEE International Symposium on Biomedical Imaging: Nano to Macro (IEEE Cat No. 04EX821)*. pp 1223–1226

Farrens S., Mboula F. N., Starck J.-L., 2017, *Astronomy & Astrophysics*, 601, A66
 Harman Z. T., Marcia R. F., Willett R. M., 2011, *IEEE Transactions on Image Processing*, 21, 1084
 He K., Zhang X., Ren S., Sun J., 2016, in *Proceedings of the IEEE Conference on Computer Vision and Pattern Recognition (CVPR)*.
 Ikoma H., Broxton M., Kudo T., Wetzstein G., 2018, *Scientific reports*, 8, 1
 Ivezić Ž., et al., 2019, *The Astrophysical Journal*, 873, 111
 Kaiser N., Squires G., Broadhurst T., 1994, arXiv preprint astro-ph/9411005
 Li X., Katayama N., Oguri M., More S., 2018, *Monthly Notices of the Royal Astronomical Society*, 481, 4445
 Lucy L. B., 1974, *The astronomical journal*, 79, 745
 Mandelbaum R., 2018, *Annual Review of Astronomy and Astrophysics*, 56, 393
 Mandelbaum R., Lackner C., Leauthaud A., Rowe B., 2012, *COSMOS real galaxy dataset*, doi:10.5281/zenodo.3242143, <https://doi.org/10.5281/zenodo.3242143>
 Mandelbaum R., et al., 2015, *Monthly Notices of the Royal Astronomical Society*, 450, 2963
 Nammour F., Schmitz M. A., Mboula F. M. N., Starck J.-L., Girard J. N., 2021, *Journal of Fourier Analysis and Applications*, 27, 1
 Nammour F., Akhaury U., Girard J., Lanusse F., Sureau F., Ali C. B., Starck J.-L., 2022, *Astronomy & Astrophysics*
 Peterson J., et al., 2005, in *American Astronomical Society Meeting Abstracts*. pp 26–23
 Richardson W. H., 1972, *JoSA*, 62, 55
 Rowe B., et al., 2015, *Astronomy and Computing*, 10, 121
 Sanghvi Y., Gnanasambandan A., Chan S. H., 2022, in *ICASSP 2022-2022 IEEE International Conference on Acoustics, Speech and Signal Processing (ICASSP)*. pp 1576–1580
 Stroke G. W., Zech R. G., 1967, *Physics Letters A*, 25, 89
 Sureau F., Lechat A., Starck J.-L., 2020, *Astronomy & Astrophysics*, 641, A67
 Terry S. K., et al., 2022, *AIROPA IV: Validating Point Spread Function Reconstruction on Various Science Cases*, doi:10.48550/ARXIV.2209.05489, <https://arxiv.org/abs/2209.05489>
 Wiener N., 1949, *Extrapolation, interpolation, and smoothing of stationary time series: with engineering applications*. MIT Press
 Yanny K., et al., 2020, *Light: Science & Applications*, 9, 1

This paper has been typeset from a \LaTeX file prepared by the author.